Validation of a numerical method for interface-resolving simulation of multicomponent gas-liquid mass transfer and evaluation of multicomponent diffusion models

Mino Woo[a], Martin Wörner[a*], Steffen Tischer[a], Olaf Deutschmann[a,b]

[a] Institute of Catalysis Research and Technology, Karlsruhe Institute of Technology (KIT), Engesserstr. 20, 76131 Karlsruhe, Germany

[b] Institute for Chemical Technology and Polymer Chemistry, Karlsruhe Institute of Technology (KIT), Engesserstr. 20, 76131 Karlsruhe, Germany

Keywords: Numerical simulation; Interfacial mass transfer; Multicomponent diffusion; Effective diffusivity model

[*] Corresponding author, Email address: martin.woerner@kit.edu, Phone: +49 721 608 47426, Fax: +49 721 608 44805

Abstract

The multicomponent model and the effective diffusivity model are well established diffusion models for numerical simulation of single-phase flows consisting of several components but are seldom used for two-phase flows so far. In this paper, a specific numerical model for interfacial mass transfer by means of a continuous single-field concentration formulation is combined with the multicomponent model and effective diffusivity model and is validated for multicomponent mass transfer. For this purpose, several test cases for one-dimensional physical or reactive mass transfer of ternary mixtures are considered. The numerical results are compared with analytical or numerical solutions of the Maxell-Stefan equations and/or experimental data. The composition-dependent elements of the diffusivity matrix of the multicomponent and effective diffusivity model are found to substantially differ for non-dilute conditions. The species mole fraction or concentration profiles computed with both diffusion models are, however, for all test cases very similar and in good agreement with the analytical/numerical solutions or measurements. For practical computations, the effective diffusivity model is recommended due to its simplicity and lower computational costs.

1 Introduction

In recent years, there has been a notable progress in the development of numerical methods for interface-resolving simulations of gas-liquid two-phase flows [1, 2]. These methods allow studying transport phenomena within the phases and across the interface numerically and offer the opportunity to acquire detailed insights into transport processes in reactive gas-liquid flows. These models and simulations can support the development and optimization of technical devices, e.g. in micro process engineering [3-5]. At small scales, diffusion may become dominant and its adequate modeling is thus a prerequisite for accurate simulation of transport phenomena in micro reactors operated at low Péclet numbers.

Numerical methods for interface-resolving simulations of two-phase flows such as the volume-of-fluid method [6], the level-set method [7] and the front-tracking method [8] rely on the single-field formulation of the Navier-Stokes equation. For simulation of interfacial mass transfer, these methods must be combined with a transient transport equation for each chemical species. Corresponding numerical methods suffer from two difficulties, namely (i) the concentration jump at the interface (which results from the different species solubility in both phases) and (ii) thin boundary layers with large concentration gradients normal to the interface. To resolve the difficulty concerning the concentration jump, two different approaches exist essentially. In the so-called two-field (or two-scalar) approach, a separate concentration equation is solved for each phase [9-13]. For this purpose, two concentration fields are employed which are set to zero when continued into the other phase. In the single-field approach, in contrast, one single concentration equation is solved for each species, which is valid in the entire domain. Here, one can distinguish

between methods that numerically preserve the discontinuity of the concentrations at both sides of the interface [14-16] and methods that solve for a transformed concentration field which is continuous at the interface [17-21]. A discussion of the advantages and disadvantages of the different concepts is provided in Deising et al. [16].

In the literature, the application of the above numerical methods is often restricted to the mass transfer of one single dilute species or to the evaporation of a pure liquid where the gas phase is a binary mixture of air and the vapor of the liquid phase [22, 23]. In other applications, the evaporation of a binary liquid mixture adjacent to vapor mixture of the same components is considered [24]. In all these cases, Fick's law with a constant or temperature dependent binary diffusion coefficient can describe the diffusion process. In chemically reacting flows, however, multiple species are involved and for each species a separate advection-diffusion-reaction equation needs to be solved to determine the local instant concentration. In mixtures with more than two species, the diffusion of a species is influenced not only by its own concentration gradient, but also by the concentration profiles of the other species. In such multicomponent mixtures, complex interactions between diffusing components (so-called cross effects) may occur [25, 26] which can only be described by multicomponent diffusion concepts.

A brief review of the relevant work on multicomponent diffusion theory is provided by Bird et al. [27]. Historically, there are two major formulations for the mass-flux relations due to diffusion in a n-component mixture. In the generalization of Fick's law (GFL) the mass flux is written as a linear combination of concentration gradients while in the Maxwell-Stefan (MS) equations, which can be considered as the most fundamental model for the description of material

transport in multicomponent system, the concentration gradient is given as a linear combination of the mass fluxes [28]. Both formulations lead to different $n \times n$ diffusivity matrices which are, however, convertible [28-30].

The GFL form has the advantages that it is easily combined with mass balances and can be directly used with standard computational fluid dynamic (CFD) routines [31]. In engineering CFD computations, usually only $n-1$ species balance equations are solved while the concentration or mass fraction of component n (the solvent) is determined from an overall material balance [32, 33]. This leads to a $(n-1)\times(n-1)$ matrix of diffusion coefficients which is in general asymmetric and dependent on composition. Except for ideal gas mixtures, there is no accepted way of estimating these coefficients other than by exhaustive experimentation [32, 34]. In the MS equations, instead, the well-documented binary diffusivities appear, though there is no a priori reason to assume this [27]. A remedy for determining the elements of the $(n-1)\times(n-1)$ GFL diffusivity matrix is therefore the inversion of the respective matrix of MS diffusivities [26, 35, 36]. This approach is denoted here as the (GFL) multicomponent model and is widely used in analytical studies as well as in numerical applications [37].

To avoid the matrix inversion of the multicomponent diffusion model, the effective diffusivity model was developed [38]. It is also called dilute approximation model [25, 39] or mixture-averaged diffusion model [40]. Though this model has limitations due to a violation of the overall mass conservation [25], it is widely used in numerical simulations [41-44] especially for dilute conditions. Some studies in catalytic combustion applications report that the effective diffusivity

model is sufficiently accurate [39, 45], while other studies report that omitting multicomponent diffusion causes significant errors [46], e.g. in combustion simulations of laminar flames [47].

In addition to the references on gaseous single-phase mass transfer in the previous paragraph, there exist a limited number of studies where the multicomponent or effective diffusivity models are employed for interfacial mass transfer in two-phase systems. Kenig and coworkers developed a mathematical model for calculation of heat and mass transfer with reaction in a laminar falling liquid film [48]. The model was verified by comparison with numerical and linearized analytical approaches [49]. Furthermore, a general analytical solution is derived for an unsteady (linearized) multicomponent diffusion-reaction problem in terms of the film model [50]. However, in the numerical examples of references [48, 50] the elements of the diffusion matrix are constant and do not depend on composition. In a CFD study with COMSOL Multiphysics, the effective diffusivity model is used to investigate multicomponent mass transfer in liquid-liquid extraction in a micro-extractor for the standard system water/toluene/acetone/metyl-isopropylketone [51]. The aqueous and organic phases are in a laminar counter-current flow and separated by a stationary flat interface. Since the latter coincides with grid cell boundaries, the exact local conditions for thermodynamic equilibrium and the component flux continuity at the interface can be easily applied. In interface capturing methods such as the VOF and level-set methods, the (moving) interface is not aligned with the mesh cell boundaries but divides the mesh cell volume into two subdomains. Then, in the single-field approach, a special numerical treatment of the diffusion term is necessary in order to fulfill the conditions of thermodynamic equilibrium and component flux continuity at the interface simultaneously.

Several authors applied the VOF method in FLUENT for performing detailed numerical studies on multicomponent heat and mass transfer in stratified gas-liquid flows [52-54]. Banerjee [52] and Haelssig et al. [53] use the effective diffusivity model where the binary diffusion coefficients are determined by Fullers method [55]. Cui et al. [54] instead account for cross-diffusion effects and compute the elements of the diffusion matrix via an exponential relationship in terms of mole fractions [26]. Finally, it is worth to mention that Dal'Toé et al. [56] studied cross diffusion effects in the interfacial heat and mass transfer of multicomponent droplets using the Euler-Lagrange approach in FLUENT. They found that cross diffusion effects were not significant for the mixture studied so that the effective diffusivity model can be used.

The main objective of the present paper is to validate a previously developed single-field approach for numerical simulation of interfacial mass transfer [20] for multicomponent diffusion-reaction systems where the interface position is not identical with mesh cell boundaries. This validation is a prerequisite for applying the method subsequently for full three-dimensional interface-capturing simulations of multicomponent mass transfer in two-phase flows. A second objective is to test and compare multispecies diffusion models used for single-phase (mostly gas-phase) mass transfer for gas-liquid mass transfer. For this purpose, numerical simulations with the multicomponent diffusion model and the effective diffusivity model are performed for various one-dimensional test problems and the results are compared with analytical or numerical solutions of the Maxwell-Stefan equations and/or experimental data from literature. In this paper, only static phases separated by a planar gas-liquid interface without flow (advection) are considered for comparison with known analytical and/or experimental data. This study shows that the differences

resulting from the two diffusion models are in general small. Furthermore, it sheds light on the conditions when composition-independent diffusion coefficients may be assumed.

The outline of the paper is as follows. In Section 2 the different diffusion models and the numerical method are introduced. In Section 3 result for various diffusive or diffusive-reactive test cases are presented and discussed. The paper closes with summary and conclusions in Section 4.

2 Mathematical model

2.1 Definitions and partial mass balances

Let us consider a multicomponent fluid (gas or liquid) composed of n chemical components (species). The thermodynamic state of the system is described by n partial mass densities $\rho_1,...,\rho_n$, by n partial velocities $\mathbf{u}_1,...,\mathbf{u}_n$ of the constituents (with respect to a fixed frame of reference) and by the temperature T of the mixture. This paper is restricted to isothermal conditions so that T is spatially uniform and constant in time. With regard to the various test cases considered in this paper, it is useful to introduce the governing equations in terms of both, mole fractions and concentrations. With partial molar concentration $c_i := \rho_i / M_i$ and mole fraction $x_i := c_i / c_t$, the molar-average velocity $\mathbf{u}$ and the molar diffusive fluxes $\mathbf{j}_i$ relative to $\mathbf{u}$ are given by

$$\mathbf{u} := \sum_{i=1}^{n} x_i \mathbf{u}_i \quad \text{and} \quad \mathbf{j}_i := c_i(\mathbf{u}_i - \mathbf{u}) \tag{1}$$

where

$$c_t := \sum_{i=1}^{n} c_i \quad \text{and} \quad \sum_{i=1}^{n} \mathbf{j}_i = 0 \tag{2}$$

Similarly, with mixture molar volume $\bar{V}_t := 1/c_t$ and volume fraction $\phi_i := c_i \bar{V}_i$, the volume-average velocity $\mathbf{u}^V$ and the molar diffusive fluxes relative to $\mathbf{u}^V$ are given by

$$\mathbf{u}^V := \sum_{i=1}^{n} \phi_i \mathbf{u}_i \quad \text{and} \quad \mathbf{j}_i^V := c_i (\mathbf{u}_i - \mathbf{u}^V) \tag{3}$$

where

$$\sum_{i=1}^{n} \phi_i = 1 \quad \text{and} \quad \sum_{i=1}^{n} \bar{V}_i \mathbf{j}_i^V = 0 \tag{4}$$

With these definitions, the partial mole balances can be written in terms of the mole fraction

$$c_t \left(\frac{\partial x_i}{\partial t} + \mathbf{u} \cdot \nabla x_i \right) + \nabla \cdot \mathbf{j}_i = r_i \tag{5}$$

and in terms of concentration and with respect to the volume-average velocity (see [26])

$$\frac{\partial c_i}{\partial t} + \nabla \cdot c_i \mathbf{u}^V + \nabla \cdot \mathbf{j}_i^V = r_i^V \tag{6}$$

For solving the latter set of equations, knowledge of the velocity field ($\mathbf{u}$ or $\mathbf{u}^V$) and appropriate constitutive equations for the diffusive fluxes ($\mathbf{j}_i$ or $\mathbf{j}_i^V$) as well as for the source/sink term due to homogeneous chemical reactions, (r_i or r_i^V) are required. In the sequel, only heterogeneous chemical reactions are considered and the source terms are set to zero $(r_i = r_i^V = 0)$.

2.2 Modeling multicomponent diffusion

This section summarizes constitutive equations for the diffusional fluxes in multicomponent systems. In this paper, only one-dimensional problems are considered. The diffusive flux vectors then simplify to $\mathbf{j}_i = (0, 0, j_i)^T$ and $\mathbf{j}_i^V = (0, 0, j_i^V)^T$, where j_i and j_i^V denote the diffusive fluxes

of species i in z-direction. For compact notation, we define $\mathbf{j} := \left(j_1, j_2, \ldots, j_{n-1} \right)^{\mathrm{T}}$ and $\mathbf{j}^{\mathrm{V}} := \left(j_1^{\mathrm{V}}, j_2^{\mathrm{V}}, \ldots, j_{n-1}^{\mathrm{V}} \right)^{\mathrm{T}}$.

2.2.1 Generalized Fick's law (GFL)

In binary systems ($n = 2$), Fick' law relates the diffusive flux to the composition gradient of one species via a (scalar) binary diffusion coefficient $D_{1,2} = D_{2,1} > 0$. For n constituents, only $n-1$ fluxes are independent, as j_n and j_n^{V} can be computed from the other fluxes via Eq. (2) and (4). Furthermore, only $n-1$ composition gradients are independent. The generalized Fick's law relates, therefore, $n-1$ fluxes linearly with the $n-1$ composition gradients. In matrix form, it reads

$$\mathbf{j} = -c_{\mathrm{t}} \mathbb{D} \nabla \mathbf{x} \tag{7}$$

where $\mathbf{x} = (x_1, x_2, ..., x_{n-1})^{\mathrm{T}}$ represents the column matrix of the mole fractions. The square GFL diffusivity matrix $\mathbb{D}$ is given by

$$\mathbb{D} = \begin{bmatrix} D_{1,1} & \cdots & D_{1,n-1} \\ \vdots & \ddots & \vdots \\ D_{n-1,1} & \cdots & D_{n-1,n-1} \end{bmatrix} \tag{8}$$

The off-diagonal elements of this matrix represent the cross diffusion effects. The concentration related quantities $\mathbf{c}$ and $\mathbb{D}^{\mathrm{V}} \leftrightarrow \mathbb{D}_{i,j}^{\mathrm{V}}$ are defined accordingly and the diffusion matrices can be transformed from one reference velocity frame to the other [26].

When all elements of the diffusivity matrix $\mathbb{D}$ (or $\mathbb{D}^{\mathrm{V}}$) are known, the system is closed with respect to the diffusive fluxes. As discussed in the introduction, determining the GFL diffusivity matrix is intricate as the non-diagonal matrix elements are in general non-zero with a positive or

negative sign and their values are a complicated function of composition [26, 34]. Therefore, more practical approaches are required for estimating the diffusivity matrix as discussed next.

2.2.2 Multicomponent model (MCM)

The MS equations for multicomponent systems can be written in the following $n-1$ dimensional matrix form [26]

$$\mathbf{j} = -c_{\mathrm{t}}\mathbb{B}^{-1}\mathbb{G}\nabla\mathbf{x} \tag{9}$$

The diagonal elements $B_{i,i}$ and the off-diagonal elements $B_{i,j}$ of the square matrix $\mathbb{B}$ are defined as

$$B_{i,i} = \frac{x_i}{Đ_{i,n}} + \sum_{\substack{k=1 \\ i\neq k}}^{n} \frac{x_k}{Đ_{i,k}}, \quad B_{i,j} = -x_i\left(\frac{1}{Đ_{i,j}} - \frac{1}{Đ_{i,n}}\right) \tag{10}$$

where $Đ_{i,j}=Đ_{j,i}>0$ denotes the (binary) Maxwell-Stefan diffusivity of i-component into j-component. For binary mixtures ($n=2$), the Fick's diffusivity $D_{1,2}$ and the Maxwell-Stefan diffusivity $Đ_{1,2}$ are identical for ideal fluids where only binary collisions are assumed to take place.

The matrix $\mathbb{G}$ in Eq. (9) represents the thermodynamic correction factor, which accounts for non-ideality effects. In the sequel, diffusion in ideal fluids is assumed so that $\mathbb{G}=\mathbb{I}$. Comparing Eq. (9) with Eq. (7) then yields $\mathbb{D}=\mathbb{B}^{-1}$. This relation is the basis of the (GFL) multicomponent model. It states that the elements of the diffusivity matrix $\mathbb{D}$ in the generalized Fick's law can be computed by inverting the binary Maxwell-Stefan diffusion matrix $\mathbb{B}$.

2.2.3 Effective diffusivity model (EDM)

To avoid the matrix inversion in the MCM, various forms of effective diffusivity models have been suggested as an alternative [26]. Here, we consider the limiting case when species *i* diffuses through $n - 1$ stagnant gases which leads to the model of Wilke [38]. In this case, the effective diffusion coefficients $D_{i,\mathrm{eff}}$ are obtained as

$$D_{i,\mathrm{eff}} = \frac{1 - x_i}{\sum_{\substack{j=1 \\ j \neq i}}^{n} x_j / Đ_{i,j}} \tag{11}$$

The diffusive flux of the effective diffusion model can be written as

$$\mathbf{j} = -c_{\mathrm{t}} \mathbb{D}_{\mathrm{eff}} \nabla \mathbf{x} \tag{12}$$

where

$$\mathbb{D}_{\mathrm{eff}} = \begin{bmatrix} D_{1,\mathrm{eff}} & \cdots & 0 \\ \vdots & \ddots & \vdots \\ 0 & \cdots & D_{n-1,\mathrm{eff}} \end{bmatrix} \tag{13}$$

The EDM can save computational time not only by avoiding the matrix inversion but also during the solution of the individual partial mass balance equations, because the off-diagonal elements are zero (and thus cross diffusion effects are absent).

2.3 Numerical method

One goal of this paper is the advancement of the in-house computer code TURBIT-VOF [57, 58] toward numerical simulation of *multi-species* reactive two-phase flows. So far, this code has been validated and applied only to two-phase flows with *single-species* mass transfer (with or without first order reaction) under dilute conditions [20, 59]. The code solves the non-dimensional three-

dimensional single-field Navier-Stokes equations with surface tension by a volume-of-fluid method with piecewise linear interface calculation (PLIC) on a staggered Cartesian grid [60]. Here, the hydrodynamic part of the code is not relevant since in this paper only reaction-diffusion problems are considered to test the multicomponent and effective diffusivity model. In this section, therefore, only the numerical approach for the mass transfer part of the code is detailed.

The TURBIT-VOF code solves the transient three-dimensional single-field concentration equation in a non-dimensional form. This equation is derived by summing up the volume-averaged concentration equations of each phase as detailed in Onea et al. [20]. In the sequel, quantities in the single-field formulation are marked by subscript "m" as they are representative for the phase-averaging of the two-phase mixture. The normalization is based on a reference length scale L_{ref}, a reference velocity scale U_{ref}, a reference time scale $t_{\mathrm{ref}} = L_{\mathrm{ref}} / U_{\mathrm{ref}}$ and a reference concentration c_{ref}. For the one-dimensional reaction-diffusion problems considered in this paper, the respective concentration equation for species i has the form

$$\frac{\partial C_{\mathrm{m},i}}{\partial \theta} + \frac{\partial}{\partial Z}\left(C_{\mathrm{m},i} U\right) = -\frac{1}{Pe_{\mathrm{ref}}} J^{\mathrm{V}}_{\mathrm{m},i} \tag{14}$$

where $\theta := t / t_{\mathrm{ref}}$, $Z := z / L_{\mathrm{ref}}$, $U := u^{\mathrm{V}} / U_{\mathrm{ref}}$ and $Pe_{\mathrm{ref}} := L_{\mathrm{ref}} U_{\mathrm{ref}} / D_{\mathrm{ref}}$. In Eq. (14),

$$C_{\mathrm{m},i} := \frac{f c_{\mathrm{L},i} + (1-f) H_i c_{\mathrm{G},i}}{c_{\mathrm{ref}}} \tag{15}$$

is a non-dimensional transformed and continuous two-phase mixture concentration (see below),

$$J^{\mathrm{V}}_{\mathrm{m},i} = -\frac{\partial}{\partial Z}\left(D_{\mathrm{m},i} \frac{\partial C_{\mathrm{m},i}}{\partial Z} \right) \tag{16}$$

is the non-dimensional diffusive flux formulated in the flavor of the EDM, and

$$D_{\mathrm{m},i} := f\,D_{\mathrm{L},i} + (1-f)D_{\mathrm{G},i} \tag{17}$$

is the two-phase mixture diffusivity. Here, f is the liquid volume fraction within the mesh cell. For pure liquid cells it is $f=1$, for pure gas cells it is $f=0$ while in mesh cells containing the interface, f can take any value in the range of $0<f<1$.

In Eq. (15), $c_{\mathrm{L},i}$ and $c_{\mathrm{G},i}$ denote the (mean) concentrations of species i in the liquid (L) and gas (G) phases within the mesh cell. Furthermore, $H_i := c_{\mathrm{L},i}^{\mathrm{eq}} / c_{\mathrm{G},i}^{\mathrm{eq}}$ is the ratio of concentrations on both sides of the interface at thermodynamic equilibrium (denoted here as non-dimensional Henry number). In the general case, a concentration jump occurs at the interface so that $H_i \neq 1$. Including H_i in definition (15) ensures that $C_{\mathrm{m},i}$ becomes continuous at the interface which is advantageous from a numerical point of view since concentration jumps of $C_{\mathrm{m},i}$ at the interface are avoided.

A disadvantage of the above transformed continuous concentration formulation is that special measures are required to ensure the continuity of the species mass flux across the interface for mesh cells containing both phases. In TURBIT-VOF, the method described by Onea et al. [20] is adopted for this purpose. This method is inspired by the formulations of Patankar [61] and Davidson & Rudman [62] and revises the mixture diffusivities in two-phase mesh cells as follows. Let k and $k+1$ denote the positions of two neighboring mesh cell centers in a one-dimensional problem. Then, the revised mixture diffusivity at the position of the mesh cell boundary $k+1/2$ is computed as

$$D_{\mathrm{m},i;k+1/2} = \left(F_{i;k+1/2}\,\frac{\lambda_{k+1/2}^{\;-0.5}}{D_{\mathrm{m},i;k}} + G_{i;k+1/2}\,\frac{1.5-\lambda_{k+1/2}}{D_{\mathrm{m},i;k+1}} \right)^{-1} \tag{18}$$

where

$$\lambda_{k+1/2} = \max\left[\min\left(f_k + f_{k+1}, 1.5\right), 0.5\right] \tag{19}$$

Here, it is $F_{i;k+1/2} = H_i$ for $f_k = 0$ and $0 < f_{k+1} \le 1$, and $F_{i;k+1/2} = 1$ otherwise. Similarly, it is $G_{i;k+1/2} = H_i$ for $f_{k+1} = 0$ and $0 < f_k \le 1$ and $G_{i;k+1/2} = 1$ otherwise. In [20], this formulation was validated by comparison with analytic/numerical solutions of one-dimensional transient diffusive mass transfer of a single species across a planar/cylindrical interface. In the sequel, this diffusivity revision procedure is referred to as continuous-concentration diffusivity model (CCDM) to distinguish between the mixture of phases in a mesh cell and the mixture of species within a phase.

The numerical solution of Eq. (14) requires initial conditions and boundary conditions which will be detailed below on a case-by-case basis. Here, it is noted that heterogeneous reactions are realized by the following boundary condition for the non-dimensional diffusive flux

$$\dot{S}_i = \frac{1}{Pe_{\mathrm{ref}}} J^{\mathrm{V}}_{\mathrm{m},i} \tag{20}$$

where $\dot{S}_i = \dot{s}_i / (U_{\mathrm{ref}} c_{\mathrm{ref}})$ denotes the productive or consumptive non-dimensional reaction rate of species i at the reactive wall. For the numerical solution of the concentration Eq. (14) with TURBIT-VOF, spatial derivatives are approximated by second-order central differences and an explicit third-order Runge-Kutta time integration method is employed.

Overall, the calculation procedure for multicomponent two-phase mass transfer from one time step to the next employing the effective diffusivity model can be summarized as follows:

1. Determine from the concentration fields $C_{\mathrm{m},i}$ with $i = 1,...,n-1$ at time level m the composition $\mathbf{x} = (x_1, x_2, ..., x_{n-1})^{\mathrm{T}}$ in all mesh cells. Use the liquid volume fraction field f to associate the composition in each mesh cell with the gas phase (when $f = 0$), the liquid phase

(when $f = 1$) or with both phases (when $0 < f < 1$), assuming in the latter case local equilibrium in two-phase mesh cells according to Henrys law.

2. Determine from composition $\mathbf{x} = (x_1, x_2, ..., x_{n-1})^{\mathrm{T}}$ at time level m the phase-associated effective diffusivities $D_{i,\mathrm{eff}}$ using Eq. (11)
3. Use Eq. (17) to compute from the phase-associated effective diffusivities $D_{i,\mathrm{eff}}$ the cell-centered two-phase mixture diffusivities $D_{\mathrm{m},i}$ in all mesh cells and for all species
4. Use the CCDM with Eq. (18) and (19) to compute from the cell-centered two-phase mixture diffusivities $D_{\mathrm{m},i}$ the diffusivity values at mesh cell faces
5. Solve the species transport equation Eq. (14) with the diffusive flux given by Eq. (16) for all species $i = 1, ..., n-1$ from time step m to $m+1$

3 Results and discussion

This section is divided into three parts, namely (i) mass transfer within a single phase (with two test cases), (ii) mass transfer across the interface between two phases (with three test cases) and (iii) dilution effect in a single phase (one test case). All test cases are one-dimensional problems in a domain $0 \le z \le h$. The reference length scale is $L_{\mathrm{ref}} = h$ so that $0 \le Z \le 1$. This computational domain is discretized by a uniform grid consisting of 40 mesh cells. Further reference quantities (e.g. U_{ref}) are defined implicitly by setting $Pe_{\mathrm{ref}} = 1$ if not mentioned otherwise.

For the multicomponent test cases, a ternary mixture is chosen ($n = 3$). The species are indicated by subscripts 1, 2 and 3 and the respective MS diffusivities are $Đ_{1,2}$, $Đ_{1,3}$ and $Đ_{2,3}$. The 2×2 diffusivity matrix $\mathbb{D} = \mathbb{B}^{-1}$ of the MCM has four non-zero elements ($D_{1,1}$, $D_{1,2}$, $D_{2,1}$, $D_{2,2}$),

where $D_{1,2}$ and $D_{2,1}$ represent the so-called cross-effects. For $n=3$, these diffusivities can be directly computed from the MS diffusivities [26, 35]. For the EDM, the two non-zero diagonal matrix elements ($D_{1,\mathrm{eff}}$, $D_{2,\mathrm{eff}}$) are computed by Eq. (11). For $n=3$, the concentration Eq. (14) is solved for species 1 and species 2 only, while the mole fraction of species 3 is determined from the relation $x_3 = 1 - x_1 - x_2$.

3.1 Revisiting multicomponent mass transfer within a single phase

This subsection presents results for two single-phase multicomponent problems (with and without surface reaction). The MCM and EDM are employed and compared with the solution of the MS equations. The purpose is to validate the numerical approach for a single phase before turning to two phases.

3.1.1 Ternary diffusion in a Stefan tube

As first test case, the ternary diffusion in a Stefan tube according to the experiment by Carty and Schrodt [63] is considered. In this experiment, a binary liquid mixture of acetone (1) and methanol (2) evaporates at temperature $T = 328.5\,\mathrm{K}$ and pressure $p = 9.94\times10^4\,\mathrm{Pa}$ and diffuses into the ambient air (3) which is treated as a single component. This case is a well-known example for employing the MS equations. Taylor & Krishna [26] solved the MS equations with $Đ_{1,2} = 8.48\times10^{-6}\,\mathrm{m^2/s}$, $Đ_{1,3} = 13.72\times10^{-6}\,\mathrm{m^2/s}$, and $Đ_{2,3} = 19.91\times10^{-6}\,\mathrm{m^2/s}$ by a fourth-order Runge-Kutta method and obtained for the total evaporative flux at the liquid-vapor interface the result $N_\mathrm{t} = 4.91\times10^{-3}\,\mathrm{mol/(m^2 s)}$ (see example 2.1.1 in their book). More recently, Newman [64]

solved the MS equations numerically for the same system considering the film, penetration and boundary layer models.

Fig. 1 shows a sketch of the present numerical set-up. As boundary conditions, at the liquid surface ($z = 0$) the equilibrium composition of the mixture is specified ($x_{1;0} = 0.319$, $x_{2;0} = 0.528$), while at the end of tube ($z = h = L_{\text{ref}} = 0.238\text{m}$) the mole fractions are set to $x_{1;h} = x_{2;h} = 1 - x_{3;h} = 0$. To account for the non-zero total molar flux, a constant and uniform molar-average velocity $u = N_{\text{t}} / c_{\text{t}}$ is specified in the convective term of the species mole fraction Eq. (5) in the entire computational domain. Here, the total concentration is computed from the ideal gas law as $c_{\text{t}} = p/(RT) = 36.4\,\text{mol/m}^3$ so that $u = 0.135\,\text{mm/s}$. For this test case $Pe_{\text{ref}} = 0.238$ is used and a mesh dependency test is conducted. The maximum variation of the results for 20, 40, 60 and 80 mesh cells is only 0.1%, both for MCM and EDM. In the sequel, the results obtained with 40 mesh cells are presented.

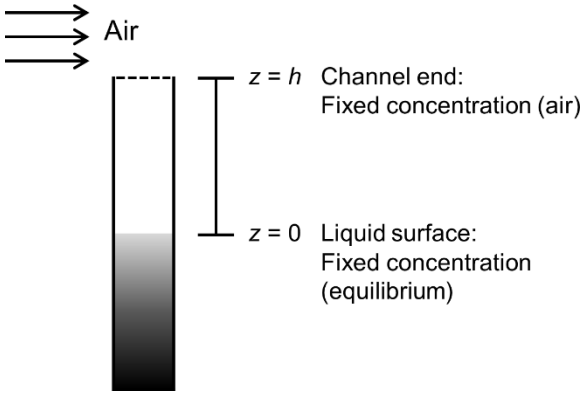

Fig. 1: Schematic diagram for the Stefan diffusion example (adopted from [26])

Fig. 2 shows a comparison of the mole fractions computed with the MCM and the EDM with the experimental data of Carty and Schrodt [63] and a numerical solution of the MS equations (see Appendix A). The MCM and EDM results are both in excellent agreement with the solution of the MS equations and are in reasonable good agreement with the experimental data. Also, the differences between the mole fraction profiles of both diffusion models are in general very small; the largest differences occur for air in the range $0.1 < Z < 0.5$ but are still below 2.3% for the MCM and below 4.3% for the EDM. Thus, the difference between both diffusion models is not significant and the EDM gives good results with lower computational cost. This result is in agreement with studies on multicomponent diffusion in other single phase test cases [39, 45].

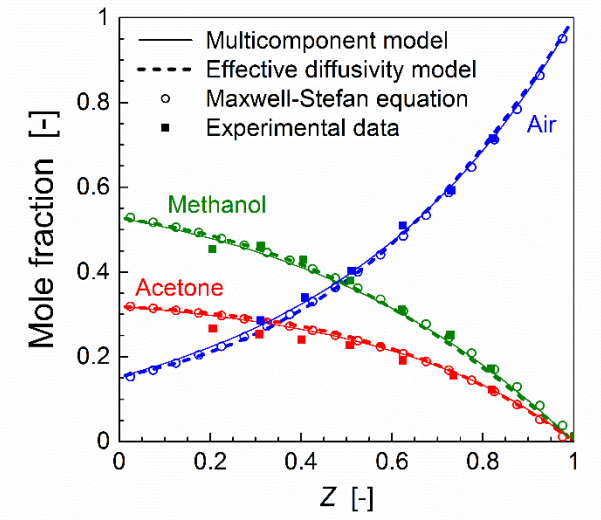

Fig. 2: Comparison of computed mole fraction profiles for the multicomponent and effective diffusivity model with experimental data [63] and numerical solution of the MS equations

In Fig. 3, the profiles of the elements of the diffusivity matrix are displayed for both diffusion models. The comparison of the diagonal matrix elements of both models reveals two points. First, the difference between both models depends on the species composition. The differences between

the diagonal diffusivities $D_{1,1}$ and $D_{1,\text{eff}}$ as well as between $D_{2,2}$ and $D_{2,\text{eff}}$ are largest at the gas-liquid interface ($Z = 0$), gradually decreases along the Z-axis and becomes virtually zero for $Z > 0.95$. The values of the off-diagonal diffusivities of the MCM are largest at the gas-liquid interface as well and drop to zero as Z approaches unity. To explore this behavior, the diffusivity profiles in Fig. 3 are compared with the mole fraction profiles in Fig. 2. In the left part of the domain, the mole fractions of acetone and methanol are higher than the mole fraction of air, while in the right part the mole fractions of acetone and methanol are much smaller than that of air. Thus, the difference between the diagonal elements of the diffusion matrix of both models is large in that part of the domain where the species mole fractions are higher than the mole fraction of the carrier species, and diminishes in regions where the acetone and methanol mole fractions are quite low so that both species can be considered as dilute. This prominent effect of the state of dilution is further investigated in Section 3.3.

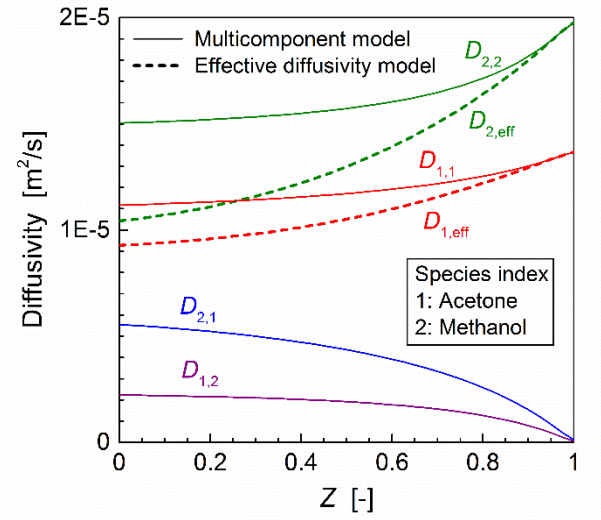

Fig. 3: Diffusivities of multicomponent model and effective diffusivity model for the Stefan tube example

The second notable point is that the local mole fractions computed by the two diffusion models are very similar even if the difference in the diagonal elements of the diffusivity matrix is quite large. Here, one may estimate the (binary) Péclet number as $Pe_{i,j} := L_{\mathrm{ref}} u / Đ_{i,j}$, which characterizes the ratio of convective and diffusive mass transport. The respective values for the three species pairs are $Pe_{1,2} = 3.79$, $Pe_{1,3} = 2.34$ and $Pe_{2,3} = 1.61$. All these values are larger than unity which indicates that convection predominates diffusion. One may thus conclude that differences in the diffusivities do not significantly affect the species mole fraction profiles in dilute conditions when diffusion is not the predominant mechanism.

3.1.2 Ternary diffusion with heterogeneous reaction

The second test case is a reaction-diffusion problem for three species for which an analytic solution of the MS equations is available [25]. The three species are CO_2 (1), O_2 (2) and CO (3). This test case describes the mass transfer to a catalytic solid surface where CO oxidation takes place by a one-step reaction $2CO + O_2 \rightarrow 2CO_2$ with arbitrary rate constant. A sketch of the computational domain and boundary conditions is depicted in Fig. 4. At the left boundary ($z = 0$) constant mole fractions ($x_{1;0} = 0.1$, $x_{2;0} = 0.2$) are specified whereas for the right wall ($z = h = L_{\mathrm{ref}} = 1\,\mathrm{mm}$) a flux condition is used. There, the molar flux for CO_2 production is specified as $N_1 = -0.1\,\mathrm{mol/(m^2 s)}$ and the molar fluxes for consumption of the other two species are obtained by stoichiometry $2N_2 = N_3 = -N_1$. The total molar flux consumed at the catalytic wall is $N_{\mathrm{t}} = N_1 + N_1 + N_3 = -0.5N_1$. These molar fluxes can be used to solve the MS equations.

The binary diffusivities for three species pairs are calculated from the kinetic theory [25]. The estimated MS diffusivities at a temperature of $300\,\mathrm{K}$ and a pressure of $1.013\times10^5\,\mathrm{Pa}$ are

$Đ_{1,2}=1.526\times10^{-5}\,\mathrm{m^2/s}$, $Đ_{1,3}=1.528\times10^{-5}\,\mathrm{m^2/s}$, and $Đ_{2,3}=2.064\times10^{-5}\,\mathrm{m^2/s}$. Since the values of $Đ_{1,2}$ and $Đ_{1,3}$ are almost the same, we follow Bird et al. [25] and set $Đ_{1,2}=Đ_{1,3}=1.528\times10^{-5}\,\mathrm{m^2/s}$. Thus, the binary diffusivity for CO and CO_2 is assumed to be same as that for O_2 and CO_2. The advantage of this assumption is that the MS equations can then be solved analytically. The corresponding steady analytical mole fraction profiles are [25]

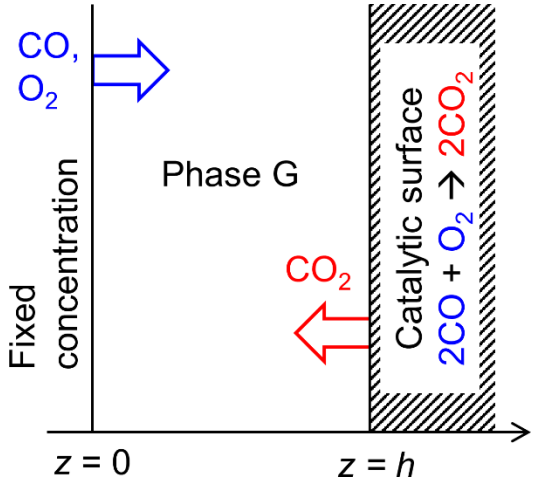

Fig. 4: Sketch of the single phase reaction-diffusion problem with one-step surface reaction

$$x_1 = -2 + (x_{1;0} + 2)\exp\left(-\frac{N_1 z}{2c_t Đ_{1,2}}\right) \tag{21}$$

$$x_2 = 1 - \frac{1}{3}(x_{1;0} + 2)\exp\left(-\frac{N_1 z}{2c_t Đ_{1,2}}\right) - \left(\frac{1}{3} - x_{2;0} - \frac{1}{3}x_{1;0}\right)\exp\left[-\left(\frac{3}{2}\frac{Đ_{1,2}}{Đ_{2,3}} - 1\right)\frac{N_1 z}{c_t Đ_{1,2}}\right] \tag{22}$$

Since the total molar flux for this second test case is non-zero as well, the numerical simulation is again obtained by specifying a constant and uniform velocity in the convective term of the

species mole fraction Eq. (5). Here, the respective value of the molar-average velocity in the entire computational domain is $u = N_t / c_t = 1.23\,\text{mm/s}$. Using the definition of the molar flux

$$N_i = c_i u + j_i = N_t x_i + j_i \tag{23}$$

the boundary conditions at $Z = 1$ are specified as

$$j_1 = \dot{s}_1 = N_1 - N_t x_1 = N_1\left(1 + \frac{1}{2}x_1\right), \qquad j_2 = \dot{s}_2 = N_2 - N_t x_2 = \frac{1}{2}N_1\left(x_2 - 1\right) \tag{24}$$

Fig. 5 compares the steady numerical results employing the MCM and EDM for the mole fraction profiles with the solution of the MS equations given by Eq. (21) and (22). For the EDM, results are additionally shown for the general case $Đ_{1,2} = 1.526 \times 10^{-5}\,\text{m}^2/\text{s} \neq Đ_{1,3}$ which have been obtained by the DETCHEM^{TM} code [65]. The purpose of this simulation is to crosscheck the implementation of the EDM in TURBIT-VOF and to quantify the effect of the assumption $Đ_{1,2} = Đ_{1,3}$. The results of the MCM are in excellent agreement with the analytical solution of the MS equations. The same holds for the EDM with the simplifying assumption $Đ_{1,2} = Đ_{1,3}$ in the region $Z < 0.5$ while for $Z > 0.5$ slight deviations occur for O_2 and CO_2. The reason is that the diffusivities from both models depend on the composition, see below. Nevertheless, also for this test case the results of both diffusion models are in reasonable good compliance with the analytic solution of the MS equations. The comparison of the results of the EDM with and without simplifying assumption shows that the mole fraction profiles for O_2 are almost identical while for CO_2 and CO differences of up to 4.9% and 2.3% occur at $Z = 1$, respectively.

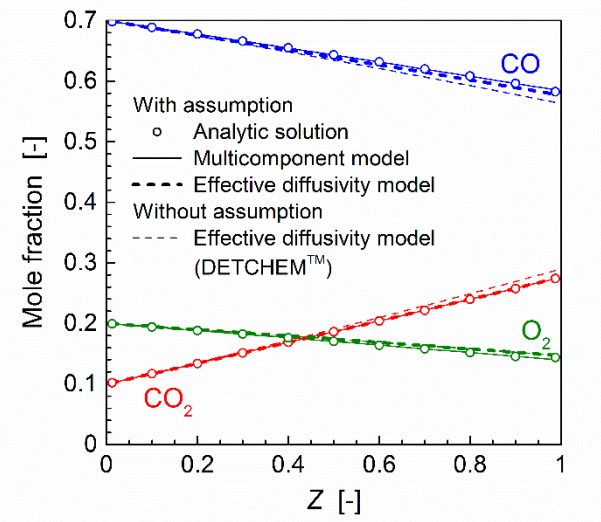

Fig. 5: Steady mole fraction profiles for the single-phase reaction-diffusion example. Comparison of results of the multicomponent model and effective diffusivity model (with and without assumption $Đ_{1,2}=Đ_{1,3}$) with the analytical solution of the MS equation

Fig. 6 shows the comparison of the profiles of the elements of the diffusivity matrix for the MCM and the EDM. For CO_2 the diffusivities $D_{1,1}$ and $D_{1,\mathrm{eff}}$ are the same because of the assumption. Furthermore, the cross-coefficient diffusivity $D_{1,2}$ is zero. The diffusivity matrices in the MCM and EDM with simplifying assumption are thus identical and so are the mole fraction profiles of CO_2. However, for the EDM without assumption, the diffusivity of CO_2 differs from $D_{1,1}$ of the MCM which causes the different mole fraction profile of CO_2 in Fig. 5. Concerning O_2, the profiles of the diffusivities $D_{2,\mathrm{eff}}$ for the two EDMs (with and without simplifying assumption) and the profile of $D_{2,2}$ for the MCM are almost identical. The slight differences in the mole fraction profiles for O_2 in Fig. 5 between the two EDMs and the MCM are thus only due to the cross-coefficient diffusivity $D_{2,1}$. The values of the binary Péclet numbers for this test case are $Pe_{1,2} = Pe_{1,3} = 0.08$ and $Pe_{2,3} = 0.06$. These data are much smaller than unity which means that the convective flux (which occurs due to a non-equimolar reaction in this example) is smaller than the

diffusive flux. It is remarkable that the difference of diffusivity does not significantly affect the mass transfer on a macro scale.

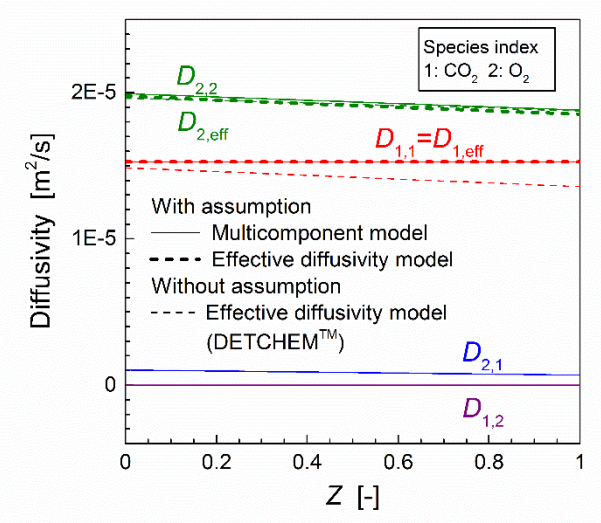

Fig. 6: Diffusivity profiles for the single phase reaction-diffusion example. Comparison of multicomponent model and effective diffusivity model with and without assumption $Đ_{1,2}=Đ_{1,3}$

3.2 Mass transfer across a planar gas-liquid interface

In this section, three test cases with mass transfer across a planar gas-liquid interface are considered. In the first two test cases, the continuous-concentration diffusivity model (CCDM) for interfacial mesh cells in TURBIT-VOF is validated for a binary mixture. In the third test case, the MCM and the EDM are employed for a ternary mixture. The second and third test cases involve a heterogeneous chemical reaction. In all three test cases the phase interface is located in the middle of the one-dimensional computational domain as shown in Fig. 7. This domain can be considered to represent a part of liquid film region in Taylor flow, in which the mass transfer occurs from the gas to the liquid phase towards a potentially reactive wall [66]. For all three test cases it is $u^{\mathrm{V}} = 0$ so that the convective term in the concentration Eq. (14) disappears.

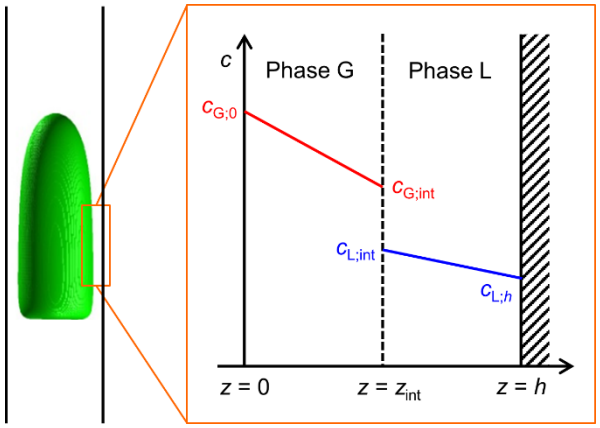

Fig. 7: Sketch for test cases on two-phase mass transfer across the interface

3.2.1 Validation of continuous-concentration diffusivity model for transient mass transfer

To investigate the accuracy of the continuous-concentration diffusivity model (CCDM) of Onea et al. [20] for transient pure diffusive mass transfer across a phase-interface (cf. Section 3.2), we revisit one test case of that paper where a time-dependent analytical solution is available for comparison. For the initial conditions of a uniform concentration $c_{G;0} = c_{ref} = 1\text{mol/m}^3$ in the gas phase ($0 < z < z_{int}$) and zero concentration in the liquid phase ($z_{int} < z < h$), the analytic solution for $C := c / c_{ref}$ in an infinite one-dimensional domain reads [67]

$$C = \begin{cases} \dfrac{1 + H\sqrt{D_L / D_G}\,\operatorname{erf}\left[(z_{int} - z)/(2\sqrt{D_G t})\right]}{1 + H\sqrt{D_L / D_G}} & \text{for} \quad z < z_{int} \\ \dfrac{H\,\operatorname{erfc}\left[(z - z_{int})/(2\sqrt{D_L t})\right]}{1 + H\sqrt{D_L / D_G}} & \text{for} \quad z > z_{int} \end{cases} \tag{25}$$

Note that at the interface ($z = z_{int}$) this concentration profile is discontinuous for $H \neq 1$.

For the numerical simulations, the computational domain needs to be finite. Here, the configuration displayed in Fig. 7 is used (with $h = L_{\mathrm{ref}} = 1\,\mathrm{mm}$) in combination with a gradient free boundary condition at $Z = 0$ and $Z = 1$. Starting from the above initial conditions, the concentration Eq. (14) is solved in time. To allow for a meaningful comparison with the analytical solution for the infinite domain, the simulations are stopped before the concentration values at $Z = 0$ and $Z = 1$ deviate notably from the respective initial values. In the simulations, the diffusivity in the gas phase is fixed $D_{\mathrm{G}} = 5 \times 10^{-5}\,\mathrm{m}^2/\mathrm{s}$ while the diffusivity in the liquid phase D_{L} is varied. The Henry number is unity ($H = 1$) so that for this test case the physical concentration profile is continuous at the interface for $t > 0$. The purpose of revisiting this test case is to quantify the influences of the CCDM as well as that of the interface position relative to the mesh cell boundary on the accuracy of the method. Simulations are thus performed with and without CCDM. The relative position of the interface with respect to the mesh cell boundary is quantified by the liquid volumetric fraction in the interfacial mesh cell (f_{int}) and is varied from 1 to 0.5, see the inset in Fig. 9.

Fig. 8 compares the analytical and computed concentration profiles for $f_{\mathrm{int}} = 1$ at $t = 50\,\mu\mathrm{s}$ and three different values of the diffusivity ratio $\Gamma := D_{\mathrm{G}} / D_{\mathrm{L}}$. For the diffusivity ratio $\Gamma = 1$, there is no diffusivity contrast between phases and the test case corresponds essentially to a single phase diffusion problem. For the diffusivity ratios 0.1 and 10, the time scale of diffusion is different in both phases and the concentration gradient is discontinuous at the interface. The numerical results obtained with the CCDM are in excellent agreement with the analytical solution given by Eq. (25) while the concentration profiles computed without the CCDM slightly differ from the analytical

solution for the cases where $\Gamma \neq 1$. We also checked that the results with CCDM are independent on the number of mesh cells. The maximum difference among grids with 21, 41, 61 and 81 cells is only 0.71%.

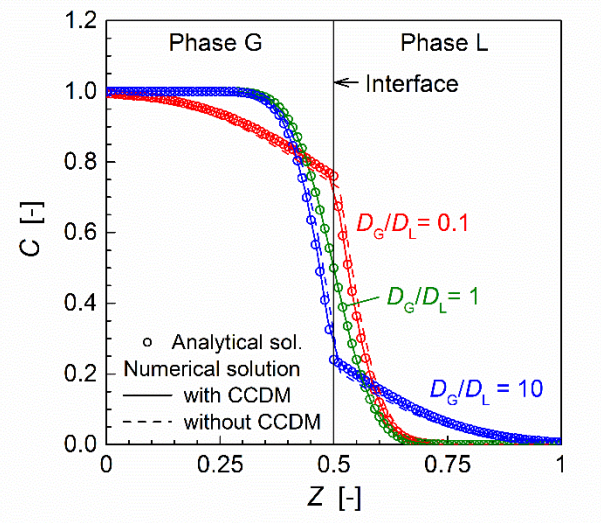

Fig. 8: Instantaneous concentration profiles for three different values of the diffusivity ratio ($H = 1$, $f_{int} = 1, t = 50\,\mu s$). Comparison of analytical solution and numerical solution with and without continuous-concentration diffusivity model (CCDM)

To study the effect of the interface position within a mesh cell, simulations for six different interface locations were performed for the diffusivity ratio $\Gamma = 0.1$. Fig. 9 shows the normalized difference between the numerical and analytic concentration profile for the simulations with and without CCDM. With CCDM, the deviation from the analytical solution is about one order of magnitude smaller than without CCDM. The largest absolute error with CCDM (0.0047 for $f_{int} = 1$) is smaller than the smallest error without CCDM (0.0134 for $f_{int} = 0.5$). For interface positions in the range of $0 < f_{int} < 0.5$, no results are shown in Fig. 9. There, the errors are smaller and the

maximum error without CCDM is 0.0124 at $f_{\mathrm{int}} = 0.1$ while the largest error with CCDM is only 0.0049 at $f_{\mathrm{int}} = 0.4$. This highlights the importance of the CCDM even for $H = 1$ when the diffusivity ratio differs from unity. Note that the increase of the deviation between numerical and analytical results, which is visible in Fig. 9 for region $0 < Z < 0.1$, originates from the zero gradient boundary condition at $Z = 0$ and is thus without relevance here.

Both with and without CCDM, the deviation from the analytical solution is smallest when the interface is located in the middle of the mesh cell and largest when the interface coincides with the mesh cell boundary. This behavior stems from the fact that in the finite volume code TURBIT-VOF the diffusivity at the cell face is needed to calculate the diffusive flux between two adjacent mesh cells. If the interface is located in the middle of the mesh cell, then the diffusivities at the cell faces are determined as the diffusivity of the respective phase. If the interface coincides with the face of two neighboring mesh cells or is close to it, then the diffusivity at this mesh face is ambiguous in the single-field formulation. In TURBIT-VOF, the respective diffusivities are estimated by the CCDM via Eq. (18).

In three-dimensional simulations, the interface orientation and the location is determined by the geometric interface reconstruction algorithm of the VOF method. The interface orientation is then hardly parallel to the cell face as in the present one-dimensional test case where the maximum error with CCDM is about 0.47%. Though the error in three-dimensional cases will be larger, it is clear that the CCDM is an indispensable ingredient of the present numerical method for an accurate simulation of interfacial mass transfer.

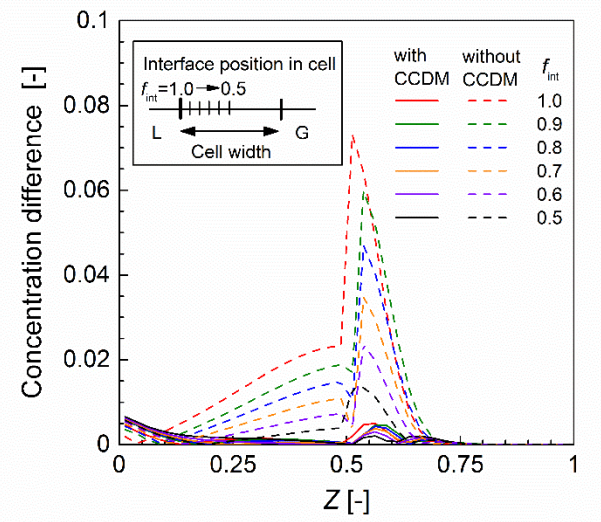

Fig. 9: Profiles of instantaneous concentration differences between analytic and numerical solution with and without CCDM for different interface locations within a mesh cell ($H = 1$, $t = 50\,\mu s$). The concentration difference is normalized by c_{ref}

3.2.2 Effect of diffusivity ratio, Henry number and reaction rate in steady state

In this test case, the reactive mass transfer of a single species across a planar interface is simulated till steady state. The numerical solution is compared with the analytical solution of a non-equilibrium stage model (NESM) where the reactor is divided in several stages [68]. Recently, this approach has been used for modelling of a dividing wall distillation column [69]. In the present work, the NESM suggested by Kenig et al. [70] is used, see appendix B. The boundary conditions combine a fixed concentration $C_m = 1$ at $z = 0$ with the flux condition $J_m^V = \dot{S} = -kC_m$ at $z = h = 1\text{mm}$. In the simulations the diffusivity ratio, the Henry number and reaction rate are varied. The lower diffusivity of the two phases is always set to $1\text{m}^2/\text{s}$.

Fig. 10 shows the concentration profiles for the diffusivity ratios 0.1, 1 and 10 at a constant reaction rate $k = 10$ m/s for $H = 1$. The numerical results are in very good agreement with those of the NESM. They show that a higher/lower diffusivity in a phase results in a lower/higher concentration gradient in that phase. An interesting result is that the concentrations at the right wall are not identical for the three diffusivity ratios even though the reaction rate is identical for all cases. The wall concentration for $\Gamma = 1$ is lower than the wall concentration for $\Gamma = 0.1$ and $\Gamma = 10$ which are identical. The reason is the different diffusive flux. For the cases with $\Gamma = 0.1$ and $\Gamma = 10$ the diffusive flux is larger as compared to the case with $\Gamma = 1$ because in the former cases the diffusivity in one phase is increased by a factor of 10.

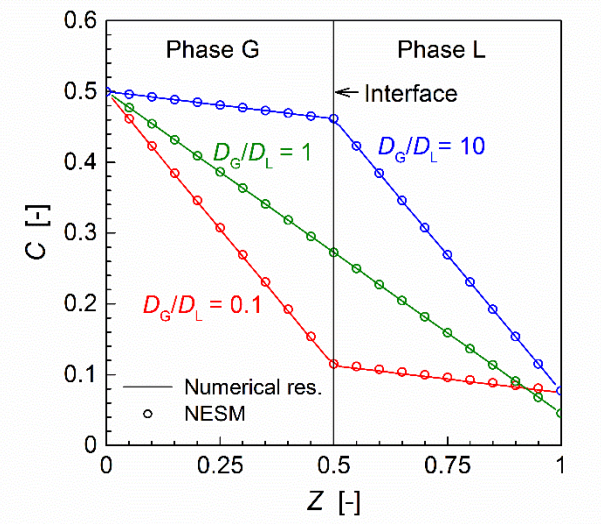

Fig. 10: Concentration profiles for steady state two-phase reactive mass transfer ($H = 1$, $k = 10$ m/s). Comparison between numerical and NESM solution for three different diffusivity ratios

The effect of the reaction rate is studied by comparing simulation results for $k = 1$ m/s and $k = 10$ m/s. In both cases the diffusivity ratio is unity and the Henry number is 0.5 so that a concentration jump occurs at the interface. The respective concentration profiles are displayed in Fig. 11, where the continuous concentration C_m is transformed back into the discontinuous physical concentration. Again, the numerical results are in very good agreement with those of the NESM. Since the diffusivity ratio is unity, the concentration gradients in both phases are identical for each case. The concentration gradient of the two cases is, however, different. The reason is that the species consumption at the reactive wall relies on the reaction rate and therefore, the diffusive mass flux and in-phase concentration gradient is higher for the case with $k = 10$ m/s than for the case with $k = 1$ m/s. From the results of these test cases, it is concluded that the CCDM is well validated for single-species interfacial mass transfer, both for transient as well as steady state conditions.

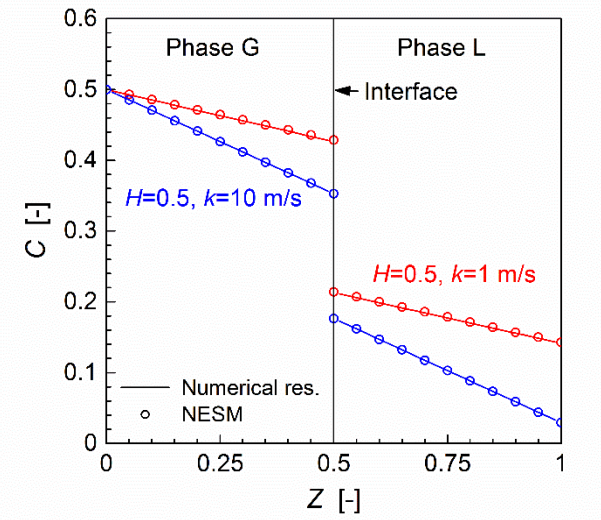

Fig. 11: Concentration profiles for steady state two-phase reactive mass transfer ($H = 0.5$, diffusivity ratio unity). Comparison between numerical and NESM solution for two different reaction rates

3.2.3 Reaction-diffusion of H_2-O_2 in water-vapor two-phase condition

The next example concerns a ternary reaction-diffusion problem across the phase interface. The three species involved are H_2 (1), O_2 (2) and H_2O (3). In the left half of the computational domain H_2O is in a gaseous state (water vapor) whereas in the right half it is in a liquid state. The temperature is 25°C and the pressure is $1.013\times10^5\,\mathrm{Pa}$. There is no phase change from gaseous to liquid H_2O or vice versa. Only H_2 and O_2 undergo mass transfer across the phase interface as they dissolve in liquid water and react at the catalytic wall to liquid H_2O. Under these conditions, there are six binary diffusivities which take the values $Đ_{1,2(G)}=Đ_{1,2(L)}=7.992\times10^{-5}\,\mathrm{m^2/s}$, $Đ_{1,3(G)}=8.068\times10^{-5}\,\mathrm{m^2/s}$, $Đ_{2,3(G)}=2.099\times10^{-5}\,\mathrm{m^2/s}$, $Đ_{1,3(L)}=4.50\times10^{-8}\,\mathrm{m^2/s}$ and $Đ_{2,3(L)}=2.10\times10^{-8}\,\mathrm{m^2/s}$, respectively [71]. The values of the Henry number of H_2 and O_2 are $H_1=52.36$ and $H_2=31.35$, respectively [72]. Thus, in this example the diffusivities in both phases differ by about three orders of magnitude and there is a large concentration jump at the interface. These features are also typical for many practical applications.

In the numerical simulation for this test case, the following boundary conditions are used. At $z=0$ the concentrations are fixed to $C_1=0.001$, $C_2=0.001$ and $C_3=0.998$, respectively. At $z=h=L_{\mathrm{ref}}=1\mathrm{mm}$ the continuity between reactive and diffusive flux is specified according to

$$\dot{S}_i=k\nu_i C_1 C_2 \tag{26}$$

The values of the stoichiometric coefficients are $-\nu_1=-2\nu_2=\nu_3$ and the reaction rate is arbitrary specified as $k=1\,\mathrm{m/s}$. For the single phase mass transfer it was concluded that the EDM is sufficiently accurate for all cases. In this test case, therefore, only the EDM is considered (in

combination with the CCDM). The steady state numerical results are compared with results of the NESM where the diffusivities are, however, evaluated with the MCM.

The profiles for H_2 and O_2 in Fig. 12 (a) show that the concentration of both species in the gas phase is almost uniform (due to the high diffusivities). At the interface, both concentrations drop dramatically according to the Henry numbers and the concentration in the liquid phase is very small. The zoom up in Fig. 12 (b) shows that the concentrations decrease toward the right wall, where the reaction takes place. Overall, the numerical results agree quite well with the results of the NESM.

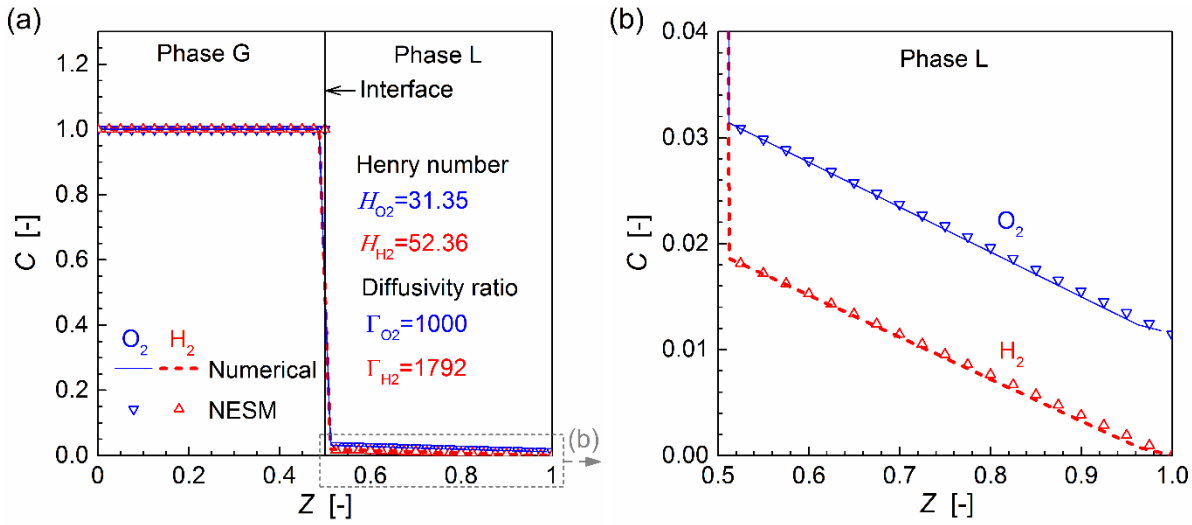

Fig. 12: Concentration profiles for two-phase reactive mass transfer of H_2-O_2-H_2O mixture. (a): entire domain, (b): zoom-up for liquid region

In Fig. 13 the profiles of the elements of the diffusivity matrix are displayed for the gas and liquid phase. This can also be regarded as a comparison between MCM and EDM under practical conditions. In each phase, the profiles of all elements of the diffusivity matrix are almost uniform. In the gas phase, H_2 and O_2 are diluted by H_2O, which lowers the composition-dependency of

the diffusivities due to the relatively small change in the species composition. In the liquid phase, the concentrations of the dissolved gas species are extremely small as compared to the H_2O concentration. These highly diluted conditions cause uniform diffusivity profiles in the liquid phase as well, with values very similar to the binary diffusion coefficients. The latter finding supports a number of studies [18, 73, 74] which use the binary diffusion coefficient directly for diffusion in the liquid phase. Nevertheless, in cases where a reaction occurs in the liquid phase which changes the composition, the EDM or even the MCM may still be essential.

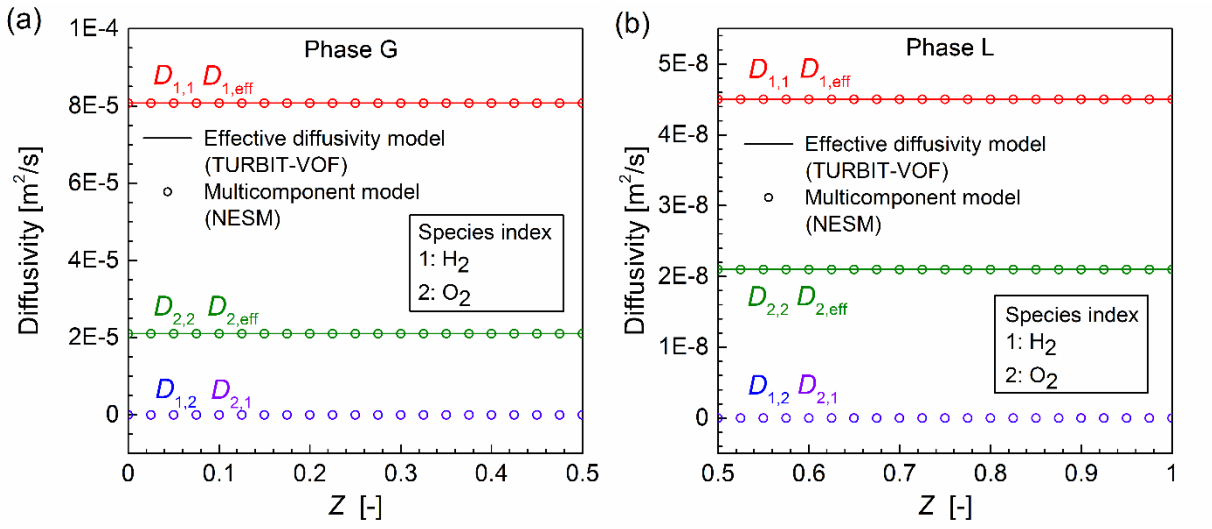

Fig. 13: Profiles of the elements of the diffusivity matrix in (a) gas phase and (b) liquid phase for H_2-O_2-H_2O mixture. Comparison of EDM (TURBIT-VOF) and MCM (NESM)

3.3 Influence of dilution

From the investigations in the previous sections, it turns out that the differences between the diffusivities of the MCM and the EDM are often negligible. Accordingly, the mole fraction and concentration profiles obtained by both diffusion models are very similar. The results for the Stefan tube (Section 3.1.1) indicate, however, that the differences in the diffusivities of both diffusion

models are very small when the mole fractions of the respective species are very small as well, but increase as the mole fractions increase. In this section, the dependency of the differences between both diffusion models on the composition of the mixture is studied therefore, in order to investigate the effect of dilution in more detail.

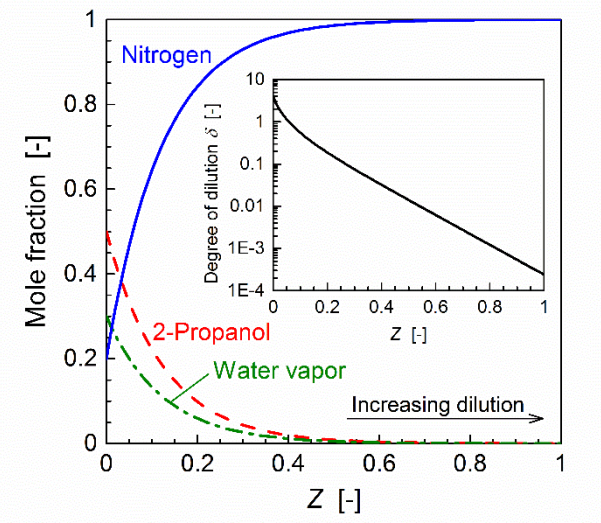

Fig. 14: Prescribed mole fraction profiles for studying the dilution effect. The inset shows the profile of the respective degree of dilution as defined by Eq. (27)

To this end, a (gaseous) single phase ternary system is considered. It consists of 2-propanol (1), water vapor (2) and nitrogen (3) which is regarded as a diluent. The gas composition is prescribed according to the non-uniform mole fraction profiles displayed in Fig. 14. The binary diffusion coefficients are taken from literature [26] and their values for the three species pairs are $Đ_{1,2}=15.99\times10^{-6}\,\mathrm{m^2/s}$, $Đ_{1,3}=14.43\times10^{-6}\,\mathrm{m^2/s}$ and $Đ_{2,3}=38.73\times10^{-6}\,\mathrm{m^2/s}$, respectively. To analyze the results in terms of dilution, a degree of dilution parameter is defined

$$\delta := \frac{1}{x_n}\sum_{i=1}^{n-1} x_i = \frac{x_1 + x_2}{x_3} \tag{27}$$

where x_n with $n=3$ here represents the carrier species in the mixture. Thus, for $\delta<1$ the mole fraction of species x_n is larger than the sum of mole fractions of all other species which can be considered as diluted. The profile of δ for the assumed composition profiles is displayed in Fig. 14 as inset.

Fig. 15 shows the diffusivities calculated from the MCM and EDM for the given mole fraction profiles. It is evident that the diagonal diffusivities of the MCM ($D_{1,1}$ and $D_{2,2}$) and the diffusivities of the EDM ($D_{1,\mathrm{eff}}$ and $D_{2,\mathrm{eff}}$) are almost identical for a wide range of the degree-of-dilution parameter. For $\delta<0.1$, the difference between the two models is very small and diffusivities from both models are hardly distinguished. Also, the cross-coefficient diffusivities ($D_{1,2}$ and $D_{2,1}$) of the MCM are almost zero in this region. As a consequence, both diffusion models will predict almost identical mole fraction profiles for dilute conditions.

Though the Stefan tube (Section 3.1.1) and the ternary reaction-diffusion examples (Section 3.1.2) are not in the diluted condition, the EDM predicts reasonable results as compared to the MCM for these test cases as well. Overall, the results of the present series of test cases provide good evidence that the EDM is sufficiently accurate with a low computational cost.

The gas-liquid test cases in the present paper are restricted to stagnant phases. In the general case with streaming phases, the velocity field of the two-phase flow is determined by solution of the Navier-Stokes equation. In the volume-averaged single-field formulation of the Navier-Stokes equations (which is used in TURBIT-VOF), the velocity has to be interpreted as center-of-mass velocity. Since it is this velocity which enters the convective term in the concentration equations,

it is of interest to estimate the difference in the various definitions of the velocity used to define the diffusive fluxes (cf. Section 2) in dependence of the dilution.

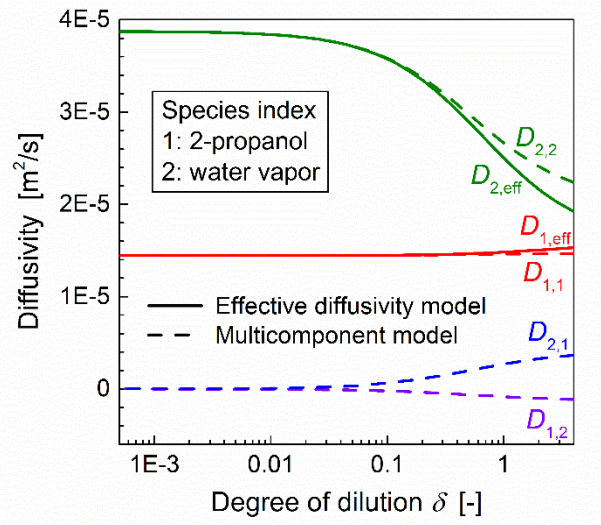

Fig. 15: Diffusivities of multicomponent model and effective diffusivity model as a function of the degree-of-dilution parameter

Besides the molar-average velocity, Eq. (1), and the volume-average velocity, Eq. (3), the mass-average velocity

$$\mathbf{u}^{\mathrm{M}} := \sum_{i=1}^{n} \omega_i \mathbf{u}_i \tag{28}$$

is often used in CFD codes, where ω_i denotes the mass fraction. While the velocities $\mathbf{u}$, $\mathbf{u}^{\mathrm{V}}$ and $\mathbf{v}$ are all identical for $n=1$, they differ for mixtures where $n \geq 2$. In this section, the prescribed mole fraction profiles from Fig. 14 are used to study the dependency of these three velocities on composition. For this purpose, the diffusive fluxes j_i are computed by the MCM with the elements of the diffusivity matrix given in Fig. 15. The total concentration is $c_{\mathrm{t}} = 40.2\,\mathrm{mol/m^3}$ where the temperature is 30°C and the pressure is $1.013\times10^5\,\mathrm{Pa}$. The component velocities are then

evaluated as $u_i = j_i / (c_t x_i)$. With the molecular species weights $m_1 = 60.1\,\mathrm{g/mol}$, $m_2 = 18.01\,\mathrm{g/mol}$ and $m_3 = 14.0\,\mathrm{g/mol}$ the mole fractions can be converted to mass fractions, and with the molar species volumes $\bar{V}_1 = 0.022\,\mathrm{m^3/mol}$, $\bar{V}_2 = 0.014\,\mathrm{m^3/mol}$ and $\bar{V}_3 = 0.011\,\mathrm{m^3/mol}$ to volume fractions. From these data, the molar-average velocity $\mathbf{u}$, the volume-average velocity $\mathbf{u}^{\mathrm{V}}$, and the mass-average velocity $\mathbf{u}^{\mathrm{M}}$ are evaluated. Fig. 16 shows the dependence of these velocities on the degree of dilution. As δ decreases, the differences between the three velocities decrease as well. For the present case, one may speculate that the differences become negligible small when δ is below about 1%. However, this statement should be considered as qualitative and a detailed quantification of the dilution effect is beyond the scope of this paper.

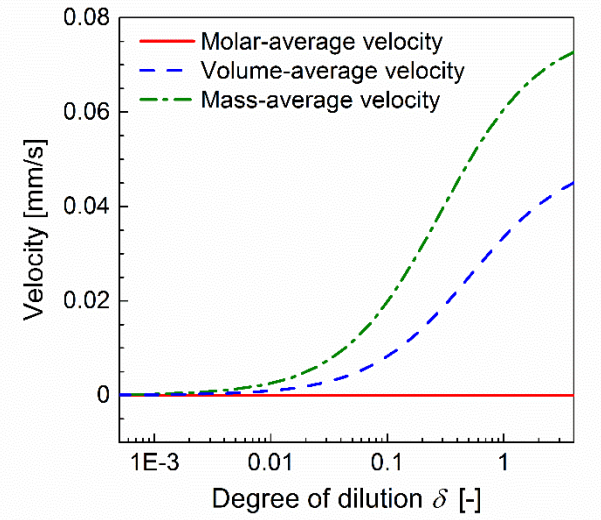

Fig. 16: Dependence of differently averaged velocities on degree-of-dilution parameter

4 Conclusions

In the present paper, multispecies single-phase and two-phase mass transfer is studied numerically, and the continuous-concentration diffusivity model (CCDM) described by Onea et al. [20] for computation of interfacial mass transfer by means of a continuous single-field concentration field is validated for multicomponent mass transfer. Transient simulations are performed for several one-dimensional non-reactive and reactive ternary test cases employing two different diffusion models in the context of Fick's generalized law, namely the multicomponent model and the effective diffusivity model. For all cases, the mole fraction or concentration profiles computed with both diffusion model are very similar and in good agreement with analytical solutions or experimental data. Since the effective diffusivity model is associated with lower computational costs, as compared to the more general multicomponent model, this model is recommended for practical computations.

Although the mole fraction and concentration profiles computed by both diffusion models are always similar, the profiles of the elements in the respective diffusivity matrix can show notable differences. The diffusivities of both models depend on the composition and the degree of dilution. For cases where the mole fractions of species undergoing mass transfer are low as compared to that of the carrier species (dilute conditions), the differences between the diffusivities of both models are low as well. The profiles of the diffusivities in the liquid phase are then almost uniform with values close to the binary diffusion coefficients.

In conclusion, the results of the present study indicate that the combination of the effective diffusivity model and CCDM is well applicable for multispecies mass transfer in gas-liquid flows.

So far, only one-dimensional test case have been considered in this paper. For two-dimensional problems, there are neither analytical solutions nor experimental data available for multicomponent diffusion with more than two species, which provide concentration field data for at least two species. The present study, nevertheless, paves the way to investigate reactive multiphase flows with multiple species under non-dilute conditions such as the Taylor flow in monolith channels with catalytic walls by two- or three-dimensional simulations.

Acknowledgment

We gratefully acknowledge the funding of this project by Helmholtz Energy Alliance "Energy Efficient Chemical Multiphase Processes" (HA-E-0004) and thank the Steinbeis GmbH & Co. KG für Technologietransfer (STZ 240 Reaktive Strömung) for a cost-free academic license of DETCHEM™.

Nomenclature

c_i	molar concentration of species i	mol/m^3
c_{ref}	reference concentration	mol/m^3
c_{t}	total molar concentration of mixture	mol/m^3
C	concentration normalized by c_{ref}	–
$D_{i,j}$	Fick diffusion coefficient in the GFL diffusivity matrix	m^2/s
$Đ_{i,j}$	Maxwell-Stefan diffusion coefficient for species pair i and j	m^2/s
$D_{i,\text{eff}}$	effective diffusivity of species i	m^2/s

f	volume fraction of liquid phase	–
H_i	Henry number of species i	–
h	length of computational domain	m
j_i	diffusive molar flux of species i relative to molar-average velocity	mol/(m^{2}s)
j_i^{V}	diffusive molar flux of species i relative to volume-average velocity	mol/(m^{2}s)
$\mathbf{j}_i$	diffusive molar flux vector of species i with molar-average velocity, $\mathbf{j}_i := (j_{i,x}, j_{i,y}, j_{i,z})^{\mathrm{T}}$	mol/(m^{2}s)
$\mathbf{j}_i^{\mathrm{V}}$	diffusive molar flux vector of species i with volume-average velocity, $\mathbf{j}_i^{\mathrm{V}} := (J_{i,x}^{\mathrm{V}}, J_{i,y}^{\mathrm{V}}, J_{i,z}^{\mathrm{V}})^{\mathrm{T}}$	mol/(m^{2}s)
$\mathbf{j}$	vector of diffusive molar flux for $n-1$ species in one-dimension with molar-average velocity, $\mathbf{j} := (j_1, j_2, \ldots, j_{n-1})^{\mathrm{T}}$	mol/(m^{2}s)
k	reaction constant	m/s
m	time step index	–
M_i	molecular weight of species i	g/mol
n	number of species	–
N	molar flux	mol/(m^{2}s)
$Pe_{i,j}$	binary Péclet number	–
Pe_{ref}	reference Péclet number	–
r_i	reactive source term of species i in Eq. (5)	mol/(m^{3}s)
r_i^{V}	reactive source term of species i in Eq. (6)	mol/(m^{3}s)
$\dot{s}_i$	reaction rate	mol/(m^{2}s)
$\dot{S}_i$	non-dimensional reaction rate	–
t	time	s
u	molar-average velocity	m/s
u_i	velocity of diffusion of species i	m/s
u^{V}	volume-average velocity	m/s
u^{M}	mass-average velocity	m/s

$\bar{V}_i$	partial molar volume of species i	m^3/mol
$\bar{V}_t$	total molar volume of mixture, $\bar{V}_t = 1/c_t$	m^3/mol
x_i	mole fraction of species i	–
z	coordinate of one-dimensional problem	m
Z	non-dimensional coordinate, $Z := z / L_{ref}$	–

Greek symbols

δ	degree of dilution	–
ν	stoichiometric coefficient	–
ρ_t	total mass density	kg/m^3
ρ_i	mass density of species i	kg/m^3
θ	non-dimensional time	–
ω_i	mass fraction of species i	–

Subscripts

eff	effective
i	species index
int	interface
G	gas phase
L	liquid phase
m	two-phase mixture quantity
ref	reference
t	total
0	initial value

Superscript

eq	equilibrium
M	mass average
V	volume average

Abbreviations

CCDM	continuous concentration diffusion model
EDM	effective diffusivity model
GFL	generalized Fick law
MCM	multicomponent model
MS	Maxwell-Stefan
NESM	non-equilibrium stage model

Appendix A. Numerical solution of Maxwell-Stefan equations

A classical model for describing diffusion in multicomponent systems is the Maxwell-Stefan diffusion, see e.g. [26]. At constant temperature and pressure, the total concentration and the binary diffusion coefficients are constant, and the driving forces of the Maxwell-Stefan diffusion are the gradients of mole fractions. For the one-dimensional problems considered here, the Maxwell-Stefan equations for ideal mixtures have the form

$$c_{\mathrm{t}} \frac{\mathrm{d}x_i}{\mathrm{d}z} = -\sum_{\substack{j=1 \\ j \neq i}}^{n} \frac{(x_i N_j - x_j N_i)}{Đ_{ij}} \tag{A.1}$$

To obtain the species distribution from the molar fluxes, the first order spatial derivative is discretized by a forward finite difference so that Eq. (A.1) is discretized at position k as

$$c_{\mathrm{t}} \frac{x_{i;k+1} - x_{i;k}}{\Delta z} = -\sum_{\substack{j=1 \\ j \neq i}}^{n} \frac{(x_{i;k} N_j - x_{j;k} N_i)}{Đ_{ij}} \tag{A.2}$$

At the left wall ($z = 0$), fixed mole fractions are specified as boundary conditions and 40 nodes are used for the Stefan-tube example of Section 3.1.1.

Appendix B. Numerical solution of non-equilibrium stage model (NESM)

Kenig et al. [70] suggested an analytical model for two-phase mass transfer in a steady state, which is based on the non-equilibrium stage model [26]. In the NESM, the reactor is divided into several stages. Between the stages, different kinds of fluxes (due to feeding, production and consumption) are transferred. Kenig et al. [70] provided the stage equation for the two-phase mass transfer with a heterogeneous model for each phase. The equations for species i in stage j for gas and liquid phases are

$$(1+r_{\mathrm{G}})\dot{V}_{\mathrm{G},i}^{j}-\dot{V}_{\mathrm{G},i}^{j+1}-\dot{V}_{\mathrm{FG},i}^{j}-J_{\mathrm{G},i}^{V,j}a_{\mathrm{int}}^{j}=0 \tag{B.1}$$

$$(1+r_{\mathrm{L}})\dot{V}_{\mathrm{L},i}^{j}-\dot{V}_{\mathrm{L},i}^{j+1}-\dot{V}_{\mathrm{FL},i}^{j}-J_{\mathrm{L},i}^{V,j}a_{\mathrm{int}}^{j}-\dot{S}_{i}^{j}a_{\mathrm{r}}^{j}=0 \tag{B.2}$$

Here, $V_{\mathrm{G},i}^{j}$ and $V_{\mathrm{L},i}^{j}$ denotes the molar flow rate to stage j with side stream, and r_{G} and r_{L} are the ratio of side stream to inter-stage flow. The second terms in Eq. (B.1) and Eq. (B.2) denote molar flow rates to stage $j+1$. The third terms represent the molar flow rates by additional feed, and the fourth terms represent the mass transfer across the gas-liquid interface (with interfacial area a_{int}^{j}). The fifth term, which appears only in the liquid phase equation, is the rate of heterogeneous reaction at the surface (with surface area a_{r}^{j}).

For the test cases presented in section 3.2, side streams and additional feeds to the stages are neglected so that $r_{\mathrm{G}}=r_{\mathrm{L}}=0$ and $V_{\mathrm{FG},i}^{j}=V_{\mathrm{FL},i}^{j}=0$. Furthermore, the one-dimensional domain is divided into a number of neighboring stages so that Eq. (B.1) and Eq. (B.2) simplify to three types of equations. For stages containing one phase only it is, depending on the phase, either

$$\dot{V}_{\mathrm{G},i}^{j}=\dot{V}_{\mathrm{G},i}^{j+1}\ \text{or}\ \dot{V}_{\mathrm{L},i}^{j}=\dot{V}_{\mathrm{L},i}^{j+1} \tag{B.3}$$

For the stage with the gas-liquid interface it is

$$\dot{V}_{\mathrm{G},i}^{j} = J_{\mathrm{G},i}^{V,j} a_{\mathrm{int}}^{j} \text{ and } \dot{V}_{\mathrm{L},i}^{j} = J_{\mathrm{L},i}^{V,j} a_{\mathrm{int}}^{j}, \tag{B.4}$$

while for the stage with the reactive surface it is

$$\dot{V}_{\mathrm{L},i}^{j} = \dot{S}_{i}^{j} a_{\mathrm{r}}^{j} \tag{B.5}$$

For the present one-dimensional problems, the interfacial area (a_{int}^{j}) and surface area of reaction (a_{r}^{j}) are assumed to be identical so that the latter equations simplify to

$$J_{\mathrm{G},i}^{V,j} = J_{\mathrm{G},i}^{V,j+1}, \; J_{\mathrm{L},i}^{V,j} = J_{\mathrm{L},i}^{V,j+1} \tag{B.6}$$

and for the stage at the right wall

$$J_{\mathrm{L},i}^{V,j} = \dot{S}_{i}^{j} \tag{B.7}$$

These equations turn out to be the same as the flux balance equation. The solution procedure is, therefore, similar as for the flux balance equation by finite difference method. The solution of this elliptic problem is obtained by an iterative method with 21 stages including one stage at the middle of the domain ($Z = 0.5$) with the gas-liquid interface, and one stage at the right reactive wall ($Z = 1$).

Conflict of interest: On behalf of all authors, the corresponding author states that there is no conflict of interest.

References

1. Tryggvason G, Scardovelli R, Zaleski S (2011) Direct numerical simulations of gas-liquid multiphase flows Cambridge University Press, Cambridge
2. Wörner M (2012) Numerical modeling of multiphase flows in microfluidics and micro process engineering: a review of methods and applications. Microfluid Nanofluid 12: 841-886
3. Günther A, Jhunjhunwala M, Thalmann M, Schmidt MA, Jensen KF (2005) Micromixing of miscible liquids in segmented gas-liquid flow. Langmuir 21: 1547-1555
4. Yue J, Luo LG, Gonthier Y, Chen GW, Yuan Q (2009) An experimental study of air-water Taylor flow and mass transfer inside square microchannels. Chem Eng Sci 64: 3697-3708
5. Haase S, Bauer T (2011) New method for simultaneous measurement of hydrodynamics and reaction rates in a mini-channel with Taylor flow. Chem Eng J 176–177: 65-74
6. Hirt CW, Nichols BD (1981) Volume of fluid (VOF) method for the dynamics of free boundaries. J Comput Phys 39: 201-225
7. Sussman M, Smereka P, Osher S (1994) A Level Set Approach for Computing Solutions to Incompressible Two-Phase Flow. J Comput Phys 114: 146-159
8. Unverdi SO, Tryggvason G (1992) A front-tracking method for viscous, incompressible, multi-fluid flows. J Comput Phys 100: 25-37
9. Bothe D, Kröger M, Alke A, Warnecke H-J (2009) VOF-based simulation of reactive mass transfer across deformable interfaces. Prog Comput Fluid Dy 9: 325-331
10. Bothe D, Kröger M, Warnecke H-J (2011) A VOF-Based Conservative Method for the Simulation of Reactive Mass Transfer from Rising Bubbles. Fluid Dyn Mater Proc 7: 303-316
11. Kenig EY, Ganguli AA, Atmakidis T, Chasanis P (2011) A novel method to capture mass transfer phenomena at free fluid-fluid interfaces. Chem Eng Process 50: 68-76
12. Bothe D, Fleckenstein S (2013) A Volume-of-Fluid-based method for mass transfer processes at fluid particles. Chem Eng Sci 101: 283-302
13. Eisenschmidt K, Ertl M, Gomaa H, Kieffer-Roth C, Meister C, Rauschenberger P, Reitzle M, Schlottke K, Weigand B (2016) Direct numerical simulations for multiphase flows: An overview of the multiphase code FS3D. Appl Math Comput 272: 508-517
14. Haroun Y, Legendre D, Raynal L (2010) Volume of fluid method for interfacial reactive mass transfer: Application to stable liquid film. Chem Eng Sci 65: 2896-2909
15. Marschall H, Hinterberger K, Schuler C, Habla F, Hinrichsen O (2012) Numerical simulation of species transfer across fluid interfaces in free-surface flows using OpenFOAM. Chem Eng Sci 78: 111-127
16. Deising D, Marschall H, Bothe D (2016) A unified single-field model framework for Volume-Of-Fluid simulations of interfacial species transfer applied to bubbly flows. Chem Eng Sci 139: 173-195

17. Petera J, Weatherley LR (2001) Modelling of mass transfer from falling droplets. Chem Eng Sci 56: 4929-4947

18. Bothe D, Koebe M, Wielage K, Prüss J, Warnecke H-J (2004) Direct numerical simulation of mass transfer between rising gas bubbles and water. In: Sommerfeld M (ed) Bubbly flows Analysis, modelling and calculation Springer, pp. 159-174.

19. Yang C, Mao Z-S (2005) Numerical simulation of interphase mass transfer with the level set approach. Chem Eng Sci 60: 2643-2660

20. Onea A, Wörner M, Cacuci DG (2009) A qualitative computational study of mass transfer in upward bubble train flow through square and rectangular mini-channels. Chem Eng Sci 64: 1416-1435

21. Hayashi K, Tomiyama A (2011) Interface Tracking Simulation of Mass Transfer from a Dissolving Bubble. J Comput Multiphase Flow 3: 247-262

22. Banerjee R (2007) A numerical study of combined heat and mass transfer in an inclined channel using the VOF multiphase model. Numer Heat Transfer, Part A 52: 163-183

23. Schlottke J, Weigand B (2008) Direct numerical simulation of evaporating droplets. J Comput Phys 227: 5215-5237

24. Hassanvand A, Hashemabadi SH (2011) Direct numerical simulation of interphase mass transfer in gas-liquid multiphase systems. Int Commun Heat Mass 38: 943-950

25. Bird RB, Stewart WE, Lightfoot EN (2002) Transport phenomena, 2nd edn John Wiley, New York

26. Taylor R, Krishna R (1993) Multicomponent mass transfer Wiley, New York

27. Bird RB, Klingenberg DJ (2013) Multicomponent diffusion-A brief review. Adv Water Resour 62: 238-242

28. Curtiss CF, Bird RB (1999) Multicomponent diffusion. Ind Eng Chem Res 38: 2515-2522

29. Matuszak D, Donohue MD (2005) Inversion of multicomponent diffusion equations. Chem Eng Sci 60: 4359-4367

30. Merk HJ (1959) The macroscopic equations for simultaneous heat and mass transfer in isotropic, continuous and closed systems. Appl Sci Res 8: 73-99

31. Gandhi KS (2012) Use of Fick's law and Maxwell-Stefan equations in computation of multicomponent diffusion. AlChE J 58: 3601-3605

32. Nauman EB, Savoca J (2001) An engineering approach to an unsolved problem in multicomponent diffusion. AlChE J 47: 1016-1021

33. Mazumder S (2006) Critical assessment of the stability and convergence of the equations of multi-component diffusion. J Comput Phys 212: 383-392

34. Rehfeldt S, Stichlmair J (2007) Measurement and calculation of multicomponent diffusion coefficients in liquids. Fluid Phase Equilibr 256: 99-104

35. Toor HL (1964) Solution of the Linearized Equations of Multicomponent Mass Transfer .1. AlChE J 10: 448-455

36. Toor HL (1964) Solution of the Linearized Equations of Multicomponent Mass Transfer .2. Matrix Methods. AlChE J 10: 460-465

37. Padoin N, Dal'Toe ATO, Rangel LP, Ropelato K, Soares C (2014) Heat and mass transfer modeling for multicomponent multiphase flow with CFD. Int J Heat Mass Transfer 73: 239-249

38. Wilke CR (1950) Diffusional Properties of Multicomponent Gases. Chem Eng Prog 46: 95-104

39. Kumar A, Mazumder S (2008) Assessment of various diffusion models for the prediction of heterogeneous combustion in monolith tubes. Comput Chem Eng 32: 1482-1493

40. Lutz AE, Kee RJ, Grcar JF, Rupley FM (1997) OPPDIF: A Fortran program for computing opposed-flow diffusion flames Sandia National Labs., Livermore, CA (United States) SAND-96-8243

41. Warnatz J, Maas U, Dibble RW (2006) Combustion: physical and chemical fundamentals, modeling and simulation, experiments, pollutant formation, 4th edn Springer, Berlin ; New York

42. Kee RJ, Coltrin ME, Glarborg P (2003) Chemically reacting flow: theory and practice Wiley-Interscience, Hoboken, N.J.

43. Hayes RE, Liu B, Moxom R, Votsmeier M (2004) The effect of washcoat geometry on mass transfer in monolith reactors. Chem Eng Sci 59: 3169-3181

44. Karadeniz H, Karakaya C, Tischer S, Deutschmann O (2013) Numerical modeling of stagnation-flows on porous catalytic surfaces: CO oxidation on Rh/Al2O3. Chem Eng Sci 104: 899-907

45. Salmi T, Warna J (1991) Modeling of Catalytic Packed-Bed Reactors Comparison of Different Diffusion-Models. Comput Chem Eng 15: 715-727

46. Kee RJ, Dixon-Lewis G, Warnatz J, Coltrin ME, Miller JA (1986) A FORTRAN computer code package for the evaluation of gas-phase, multicomponent transport properties Sandia National Labs., Livermore, CA (United States) SAND86-8246

47. Desilets M, Proulx P, Soucy G (1997) Modeling of multicomponent diffusion in high temperature flows. Int J Heat Mass Transfer 40: 4273-4278

48. Kenig EY, Kholpanov LP (1992) Simultaneous Mass and Heat-Transfer with Reactions in a Multicomponent, Laminar, Falling Liquid-Film. Chem Eng J Biochem Eng J 49: 119-126

49. Kenig EY, Butzmann F, Kucka L, Gorak A (2000) Comparison of numerical and analytical solutions of a multicomponent reaction-mass-transfer problem in terms of the film model. Chem Eng Sci 55: 1483-1496

50. Kenig EY, Schneider R, Gorak A (2001) Multicomponent unsteady-state film model: a general analytical solution to the linearized diffusion-reaction problem. Chem Eng J 83: 85-94

51. Chasanis P, Brass M, Kenig EY (2010) Investigation of multicomponent mass transfer in liquid-liquid extraction systems at microscale. Int J Heat Mass Transfer 53: 3758-3763

52. Banerjee R (2008) Turbulent conjugate heat and mass transfer from the surface of a binary mixture of ethanol/iso-octane in a countercurrent stratified two-phase flow system. Int J Heat Mass Transfer 51: 5958-5974

53. Haelssig JB, Tremblay AY, Thibault J, Etemad SG (2010) Direct numerical simulation of interphase heat and mass transfer in multicomponent vapour-liquid flows. Int J Heat Mass Transfer 53: 3947-3960

54. Cui XT, Li XG, Sui H, Li H (2012) Computational fluid dynamics simulations of direct contact heat and mass transfer of a multicomponent two-phase film flow in an inclined channel at sub-atmospheric pressure. Int J Heat Mass Transfer 55: 5808-5818

55. Poling BE, Prausnitz JM, O'Connell JP (2001) The properties of gases and liquids, 5th edn McGraw-Hill, New York

56. Dal'Toe ATO, Padoin N, Ropelato K, Soares C (2015) Cross diffusion effects in the interfacial mass and heat transfer of multicomponent droplets. Int J Heat Mass Transfer 85: 830-840

57. Sabisch W (2000) Dreidimensionale numerische Simulation der Dynamik von aufsteigenden Einzelblasen und Blasenschwärmen mit einer Volume-of-Fluid-Methode Karlsruhe, Forschungszentrum Karlsruhe Wissenschaftliche Berichte, FZKA 6478 Pages|.

58. Sabisch W, Wörner M, Grötzbach G, Cacuci DG (2001) Three-dimensional simulation of rising individual bubbles and swarms of bubbles by a volume-of-fluid method. Chem Ing Tech 73: 368-373

59. Kececi S, Wörner M, Onea A, Soyhan HS (2009) Recirculation time and liquid slug mass transfer in co-current upward and downward Taylor flow. Catal Today 147S: S125-S131

60. Öztaskin MC, Wörner M, Soyhan HS (2009) Numerical investigation of the stability of bubble train flow in a square minichannel. Phys Fluids 21: 042108 doi:10.1063/1.3101146

61. Patankar SV (1980) Numerical heat transfer and fluid flow Hemisphere Pub. Corp. ; McGraw-Hill, Washington, New York

62. Davidson MR, Rudman M (2002) Volume-of-fluid calculation of heat or mass transfer across deforming interfaces in two-fluid flow. Numer Heat Transfer, Part B 41: 291-308

63. Carty R, Schrodt T (1975) Concentration Profiles in Ternary Gaseous Diffusion. Ind Eng Chem Fundam 14: 276-278

64. Newman J (2009) Stefan-Maxwell mass transport. Chem Eng Sci 64: 4796-4803

65. Deutschmann O, Tischer S, Correa C, Chatterjee J, Kleditzsch S, Janardhanan V, Mladenov N, Minh HD, Karadeniz H, Hettel M (2014) DETCHEM^{TM} User Manual

66. Irandoust S, Ertle S, Andersson B (1992) Gas-Liquid Mass-Transfer in Taylor Flow through a Capillary. Can J Chem Eng 70: 115-119

67. Crank J (1975) The mathematics of diffusion, 2d edn Clarendon Press, Oxford, Eng

68. Krishnamurthy R, Taylor R (1985) A Nonequilibrium Stage Model of Multicomponent Separation Processes .1. Model Description and Method of Solution. AlChE J 31: 449-456

69. Hiller C, Buck C, Ehlers C, Fieg G (2010) Nonequilibrium stage modelling of dividing wall columns and experimental validation. Heat Mass Transfer 46: 1209-1220

70. Kenig E, Gorak A (1995) A Film Model-Based Approach for Simulation of Multicomponent Reactive Separation. Chem Eng Process 34: 97-103

71. Cussler EL (2009) Diffusion: mass transfer in fluid systems, 3rd edn Cambridge University Press, Cambridge; New York

72. Sander R (2015) Compilation of Henry's law constants (version 4.0) for water as solvent. Atmos Chem Phys 15: 4399-4981

73. Chasanis P, Lautenschleger A, Kenig EY (2010) Numerical investigation of carbon dioxide absorption in a falling-film micro-contactor. Chem Eng Sci 65: 1125-1133

74. Machado RM (2007) Fundamentals of Mass Transfer and Kinetics for the Hydrogenation of Nitrobenzene to AnilineALR Application Note Mettler-Toledo AutoChem. Inc.